PROCEEDINGS OF SPIE

SPIEDigitalLibrary.org/conference-proceedings-of-spie

Antenna-coupled thermal kinetic inductance detectors for ground-based millimeter-wave cosmology

Wandui, Albert, Bock, James, Frez, Clifford, Hunacek, Jon, Minutolo, Lorenzo, et al.

Albert K. Wandui, James J. Bock, Clifford Frez, Jon Hunacek, Lorenzo Minutolo, Hien Nguyen, Bryan Steinbach, Anthony Turner, Jonas Zmuidzinas, Roger O'Brient, "Antenna-coupled thermal kinetic inductance detectors for ground-based millimeter-wave cosmology," Proc. SPIE 11453, Millimeter, Submillimeter, and Far-Infrared Detectors and Instrumentation for Astronomy X, 114531E (13 December 2020); doi: 10.1117/12.2563373

SPIE.

Event: SPIE Astronomical Telescopes + Instrumentation, 2020, Online Only

Antenna-Coupled Thermal Kinetic Inductance Detectors for Ground-Based Millimeter-Wave Cosmology

Albert K. Wandui[a], James J. Bock[a,b], Clifford Frez[b], Jon Hunacek[a], Lorenzo Minutolo[a], Hien Nguyen[b], Bryan Steinbach[a], Anthony Turner[b], Jonas Zmuidzinas[a], and Roger O'Brient[b]

[a] Department of Physics, California Institute of Technology, Pasadena, CA, 91125, USA
[b] Jet Propulsion Lab, Pasadena, CA, 91109, USA

ABSTRACT

We present prototype antenna-coupled thermal kinetic inductance detectors (TKIDs) designed for Cosmic Microwave Background (CMB) observations in the 150 GHz band. The next generation of telescopes studying the CMB will require large arrays of detectors on cryogenic focal planes to achieve higher sensitivity than the current experiments. However, currently used detector technologies would achieve this advance at the cost of increased integration and readout complexity. TKIDs have demonstrated photon-limited noise performance comparable to traditional bolometers with a radio frequency (RF) multiplexing architecture that enables the large detector counts needed. We characterize TKIDs fabricated for observing the CMB in a frequency band centered at 150 GHz and discuss their optical performance. These devices are a critical step towards fielding a pathfinder *Keck* Array camera with 512 devices on a focal plane.

Keywords: TKID, bolometer, cosmic microwave background, antenna-coupled, kinetic inductance detectors

1. INTRODUCTION

The Cosmic Microwave Background (CMB) is a key observable for improving our understanding of the early universe.[1] In particular, the B-mode polarization of the CMB at degree angular scales constrains the tensor-to-scalar ratio r of primordial modes from the inflationary epoch.[2,3] Improving constraints on r requires observing the millimeter wave sky in several frequency bands in order to separate out the foregrounds due to scattering from galactic dust and synchrotron radiation.[4] Since the polarization signal is faint, experiments must deploy large arrays of sensitive bolometric detectors to build up the required sensitivity.

In current experiments, arrays of Transition Edge Sensor (TES) bolometers are used to this effect.[5] However, since TESes have a low output impedance, Superconducting Quantum Interference Devices (SQUID) amplifiers must be used to provide the impedance matching required to read out the detectors through a chain of cold and warm electronics.[6] To limit the heat load through the readout cables, TES bolometers are multiplexed using either time division multiplexing (TDM) or frequency division multiplexing (FDM). Using these techniques kilo-pixel arrays of TES bolometers have been deployed and are currently observing the CMB. The next generation of CMB instruments will require even higher detector counts. Thermal Kinetic Inductance Detectors (TKIDs) are an alternative detector technology that is intrinsically scalable to large arrays and offers the same noise performance as TES bolometers do. Each TKID consists of a superconducting resonator with a unique resonance frequency and a narrow bandwidth. Many TKID pixels can therefore be read out on a single readout line using fast Field Programmable Gate Array (FPGA) based or Graphical Processor Unit (GPU) based readout systems.[7]

In a TKID bolometer, the changes in the island temperature are tracked by monitoring the resulting change in the resonance frequency or the quality factor of the resonator. Unlike a kinetic inductance detector (KID), the detected photons do not directly break Cooper-pairs into quasiparticles in the superconductor. Rather, the optical power is thermalized on the substrate and the thermal phonons generate the quasiparticles. Integrating a superconducting resonator with a thermal bolometer circuit provides additional design flexibility since the absorber and resonator can be optimized independently.

In these proceedings, we describe the design and optical performance of antenna-coupled prototype TKIDs. In previous work,[8,9] we presented a design for a dark TKID device that demonstrated that TKIDs could offer photon noise limited

Further author information: (Send correspondence to Albert K. Wandui: Email: awandui@caltech.edu.)

Millimeter, Submillimeter, and Far-Infrared Detectors and Instrumentation for Astronomy X,
edited by Jonas Zmuidzinas, Jian-Rong Gao, Proc. of SPIE Vol. 11453, 114531E
 · doi: 10.1117/12.2563373

performance while observing the CMB in the 150 GHz band. Here, we show that our dark TKID design can be coupled with a planar lithographed phased-array antenna as the active optical element. Even though our optical TKID devices are optimized for making observations of the CMB at 150 GHz, with an expected sky Rayleigh-Jeans temperature $T_{rj} \sim 8$ K, we demonstrate that these TKIDs can perform well even at room temperature backgrounds (300 K), allowing for in lab characterization. These prototype devices are a crucial step towards a planned deployment of a full TKID focal plane in a *Keck* telescope at the South Pole.

2. DEVICE DESIGN

We designed test chips with 12 TKID devices each: 8 optically active and 4 dark devices. The resonators were defined in a frequency band starting at 250 MHz and with a 5 MHz frequency spacing. Adjacent pairs of resonators were coupled to a single dual-polarization antenna such that each optically active resonator bolometer measures the optical power from a single polarization mode of the antenna.

The antenna itself consists of a two dimensional array of closely-spaced slots in the ground plane. There are two sets of orthogonally oriented and co-located slots corresponding to the two polarization modes. This antenna design is the same as has been used in BICEP2/ *Keck* Array.[10,11] The optical power from the antenna passes through an on-chip band defining filter before being dissipated in a Au meander strip on the bolometer island. From numerical simulations and measured in-field performance, our antenna design provides spectral bands with 20% - 30% bandwidth, symmetric co-aligned beams and a low 0.5% cross-polar response. The *Keck* Array camera has $f/2.2$ refractive optics.[12] To match the antenna beam to the camera optics, the antenna is 7.8mm long on each side in a 12x12 array of slots. The beam is constructed by a uniform illumination of the slot array and the detector beam terminates at -15 dB on the cold stop of the camera at 4K

The bolometer island is fabricated from a patterned low stress silicon nitride (LSN) layer. The released island is mechanically supported on 300 μm long legs. The leg length sets the thermal conductance of the bolometer and therefore the island temperature. Our TKID design targets operation from a 250 mK bath temperature in order to achieve a 380 mK operating temperature T_o with the expected 5 pW loading from observing the millimeter wave sky in a 150 GHz band with a 25% bandwidth from the South Pole.[12] The niobium ground plane of the antenna layer extends onto the thermal island through the bolometer legs and is placed underneath the resistive meander to isolate it from the aluminum resonator inductor which is situated at the opposite end of the bolometer island. We maintain a small Au heater on the thermal island to measure thermal conductances, thermal time constants, responsivity and noise. Figure 1 shows an Scanning Electron Microscope (SEM) micrograph of the resonator bolometer with the inductor, calibration heater and resistive meander visible.

The resonator is built out of lithographed, lumped-element inductors and capacitors. In our design, the aluminum inductor and niobium main capacitor are identical for all the resonators on the chip. The resonance frequency is set during fabrication by using a pair of knife cells to blade off sections of the fingers of the inter-digitated capacitor. Smaller coupling capacitors were also used to set the coupling of the resonator to the readout line. We chose the coupling capacitors to ensure that the coupling quality factor Q_c of our devices matches the internal quality factor Q_i at the operating temperature. The thermal response of the resonator is limited to the aluminum inductor ($T_c \sim 1.2$K) on the bolometer island since the bulk of the resonator circuit is fabricated out of niobium with a much higher superconducting transition temperature, $T_c \sim 9$K.

The MUSIC KID camera fielded resonators that used inter-digitated capacitors. Their team reported that the IDC acts as a multi-moded broadband antenna creating significant response to optical power even without an antenna.[13] To remedy this, we implemented an RF choke consisting of short co-planar wave guide (CPW) and microstrip sections between the capacitor and the inductor. The choke was designed in Sonnet[14] to achieve 30 dB suppression of direct capacitor stimulation in our design band (125 - 175 GHz). In addition, a pure 50 Ω microstrip using a SiO_2 dielectric is less than 2 μm wide. On a full wafer, the feedline is long (~ 0.5 m) which is difficult to reliably fabricate with no defects or line breaks. To remedy this, we implemented a hybrid CPW-microstrip feedline with a line impedance of 50 Ω as well as a wide 8 μm main feedline that is less susceptible to catastrophic line defects. A hybrid line is desirable because a pure CPW feedline would create breaks in the ground plane of the wafer. The microstrip sections bridge the ground plane underneath the main feedline keeping the entire ground plane on the wafer continuous. Figure 2 is an SEM micrograph of the resonator capacitor and shows a section of the feedline on chip.

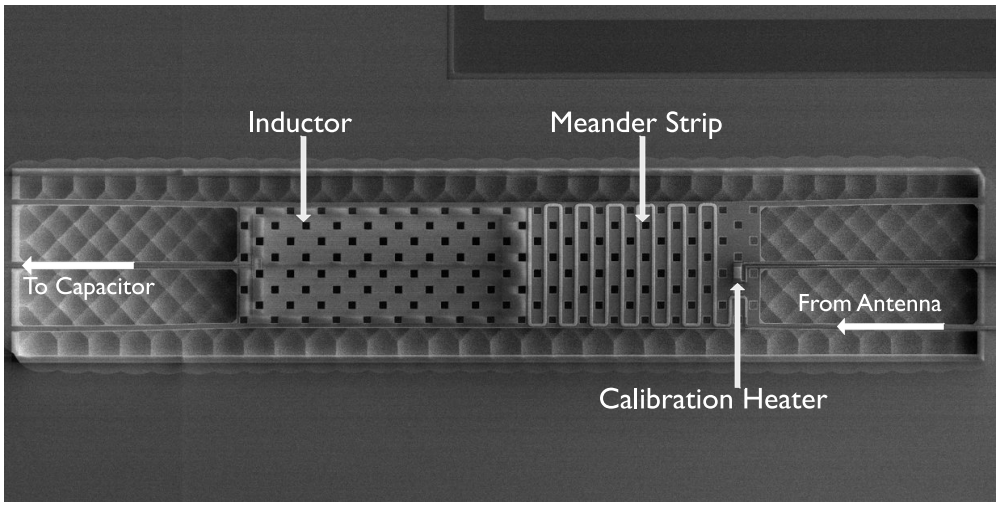

Figure 1: SEM micrograph of the TKID bolometer. The inductor and the microstrip lines that run off the island to the capacitor are visible on the left. To the right is the meander strip that terminates the microstrip line from the antenna as well as a Au heater for calibrating the bolometer response. The dense network of square holes on the island are for the XeF_2 release process that forms the island.

3. EXPERIMENTAL SETUP

We initially characterized our devices in a dark configuration in a Model 103 Rainier Adiabatic Demagnetization Refrigerator (ADR) at the Jet Propulsion Lab (JPL). With the test chip installed, the cryostat achieves an ultra-cold (UC) stage temperature of 80 mK. For the optical testing, we installed our devices in a new focal plane installed in a *Keck* Array camera at Caltech that has been fitted with RF hardware. The optical system consists of a pair of low-loss high-density polyethylene (HDPE) lenses with a refractive index $n = 1.5$ that are cooled to 4K. Unfortunately, the lenses we had available were anti-reflection (AR) coated for the 220 GHz band rather than at 150 GHz. In our target band, the optics are in effect uncoated, causing reflection loss at each of the air to dielectric interfaces. For normally incident rays, the reflectance at the air-dielectric interface is given by, $R = \left(\frac{n-1}{n+1}\right)^2 = 4\%$. Accounting for the 2 lenses, we expect the transmission to degrade by about 15%, averaged across the detectors' optical band . The implementation of the RF chain and the system level design requirements for fielding a TKID camera are given in Minutolo et. al.[15]

The test chip was mounted in an aluminum holder installed on the focal plane. The optical window of the holder is 28.6 mm on each side. The chip was held down using copper clips and a quartz microscope slide of thickness .25 mm was glued to the backside of the chip exposed by the optical window as an anti-reflection coating for the air-silicon interface. On the front side of the chip, a 0.5mm gap between the chip and the chip cover provides a $\lambda/4$ backshort for the antenna.

4. DETECTOR PERFORMANCE

Of the 12 resonators on chip, we identified 6 resonators within our design band; with 2 dark devices and 4 light devices. 2 of the optically active resonators have calibration heaters wired up for biasing externally. We also identified 5 higher frequency resonators within the 700-850 MHz band. This frequency range matches the expected location of the self resonances of the main capacitor tank found using numerical simulations.[14] These resonators are visible even above 4K, and we have identified them as niobium resonators which arise due to shorts between the capacitor fingers. In the time since the devices discussed here were fabricated, we have further improved our fabrication process to reduce the incidence of shorts between the capacitor fingers. In addition, we have also tested the use of a focused ion beam (FIB) to clear out small shorted capacitor sections to recover devices.

4.1 Resonator Properties

We characterize our resonators by measuring the forward transmission S_{21} as a function of the readout frequency for each of the resonators. S_{21} is then fit using a single pole Lorentzian model that accounts for kinetic inductance non-linearity and

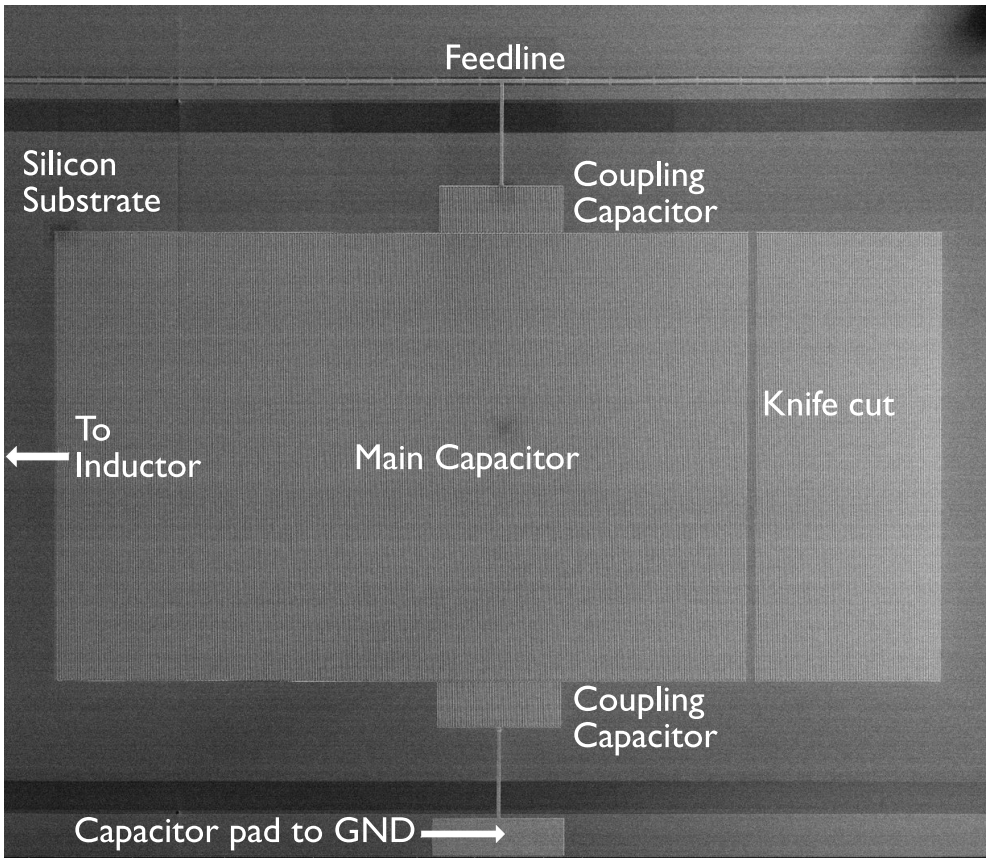

Figure 2: SEM micrograph of the TKID capacitors and feedline. The capacitors are deposited directly on the silicon substrate which is exposed in a large via through the dielectric stack of the wafer. The smaller capacitors on each side of the capacitor set the coupling of the resonator to the feedline seen at the top. The large niobium pad at the bottom of the image makes a parallel plate capacitor contact to the ground plane in place of a direct via.

resonator asymmetry.[16,17] In a dark cryostat configuration and starting from a 95 mK bath temperature, we measured the resonator quality factor as a function of the readout power in the range -110 dBm to -70 dBm. Above -80 dBm the kinetic inductance bifurcation parameter $a > 0.8$ marking the onset of the non-linearity. We also characterized our resonators under bath temperature sweeps at a -90 dBm single tone readout power level.

Using the bath temperature sweep data, we fit the frequency as a function of the bath temperature to a Mattis-Bardeen (MB) plus two-level system (TLS) model.[18] Figure 3 shows that the model describes the data well across the entire temperature range measured. As an additional step, we took the best fit parameters and used them to predict the resonator quality factors. Above 300 mK, which is the regime of interest, and where the Mattis-Bardeen dependence dominates, the best fit MB parameters predict the quality factor well. Below 250 mK, we see TLS-like behavior in Q_i. However, the loss tangent, $F\delta_0$ that is obtained from the frequency shift data is too small to match the measured Q_i. This indicates that there is an additional effect that modifies Q_i at lower temperature but that does not affect the frequency shift data. This is currently being investigated. The best fit parameters summarized in table 1 show that the resonator parameters are largely consistent from resonator to resonator.

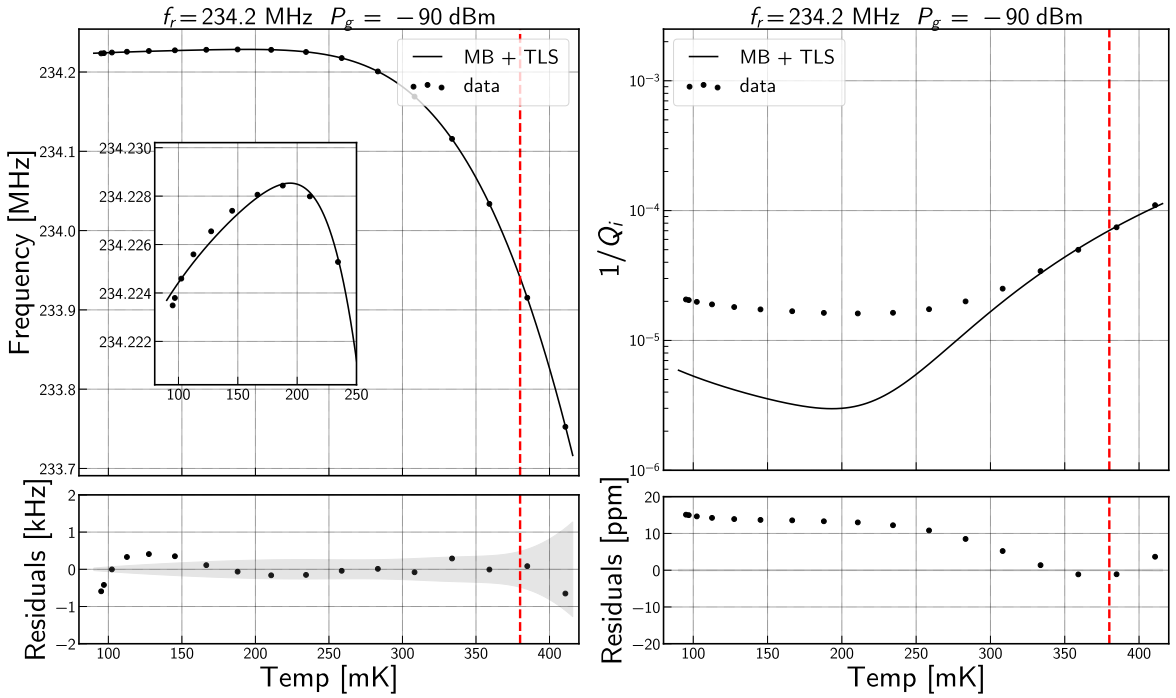

Figure 3: Fits to the frequency shift data (figure a.) for the 234.2 MHz resonator under a MB + TLS model. The inset plot has a smaller x axis range to better show the agreement between the data and the fit. The lower plot gives the residuals to the fit. The shaded region is the 1 sigma error obtained from the covariance of the best fit. The best fit parameters are summarized in table 1. In figure b, the best fit parameters obtained from fitting the frequency shift data are used to predict the quality factor. Above 300 mK, where the MB dependence dominates, the agreement between the data (black dots) and prediction (solid line) is strong.

4.2 Optical Performance

The optical efficiency is the fraction of the total incident optical power that is absorbed by the detectors on the focal plane. Losses due to reflections in the optical chain, antenna network and detectors contribute to the end-to-end optical efficiency. can measure the end-to-end optical efficiency of the optical system directly. We measured the resonator response in resonance frequency and quality factor to aperture filling blackbody sources at 77K and 300 K. The difference in the optical power ΔP from the temperature difference $\Delta T = (300\text{K} - 77\text{K})$ needed in order to infer the efficiency can be directly measured by biasing the resonators under a 77K load using the calibration heaters until the resonator response matches the response seen at a 300K load as shown in figure 4. The end to end efficiency can be calculated given the measured band center ν_0 and bandwidth $\Delta\nu$ of the device using the relation

f_r [MHz]	α_k	T_c[K]	$F\delta_0$ $[\times 10^{-5}]$
234.2	0.52 ± 0.01	1.388 ± 0.004	9.5 ± 0.4
243.1	0.54 ± 0.01	1.396 ± 0.002	8.6 ± 0.4
258.5	0.53 ± 0.01	1.397 ± 0.005	9.1 ± 0.4
264.7	0.55 ± 0.01	1.396 ± 0.005	9.6 ± 0.3
268.8	0.53 ± 0.01	1.390 ± 0.007	9.9 ± 0.5
279.6	0.53 ± 0.01	1.390 ± 0.006	9.9 ± 0.4

Table 1: Best fit Mattis-Bardeen (MB) and two-level system (TLS) parameters of the 6 TKID bolometers measured at -90 dBm. The kinetic inductance fraction, α_k and the superconducting transition temperature T_c are the 2 MB parameters while the loss tangent constant $F\delta_0$ sets the TLS effect.

$$\Delta P \approx \eta \cdot k_B \cdot \Delta T \cdot \left(\frac{\Delta \nu}{\nu_0}\right) \cdot \nu_0. \tag{1}$$

The total camera efficiency is 29% on average as given in table 2. We measured a lower $dP/dT = 0.15$ pW/K on average than is expected for our antenna design (0.17 pW/K). This difference can be accounted for by the 15% drop in transmission through the optics chain due to reflections off the uncoated optics. In addition, the microstrip lines of the antenna were fabricated using a liftoff recipe. In early antenna designs for BICEP2 and *Keck*,[10] it was empirically observed that liftoff recipes contributed to loss in the microstrip lines, presumably by leaching organic materials from the resist. This degrades the antenna performance, and the optical efficiency in particular. Etched microstrip was not observed to have these deficiencies.[10] We have switched to an etchback recipe for microstrip lines in devices currently under fabrication. We are also currently working on making direct measurements of the detector efficiency using an in-cryostat cold load.

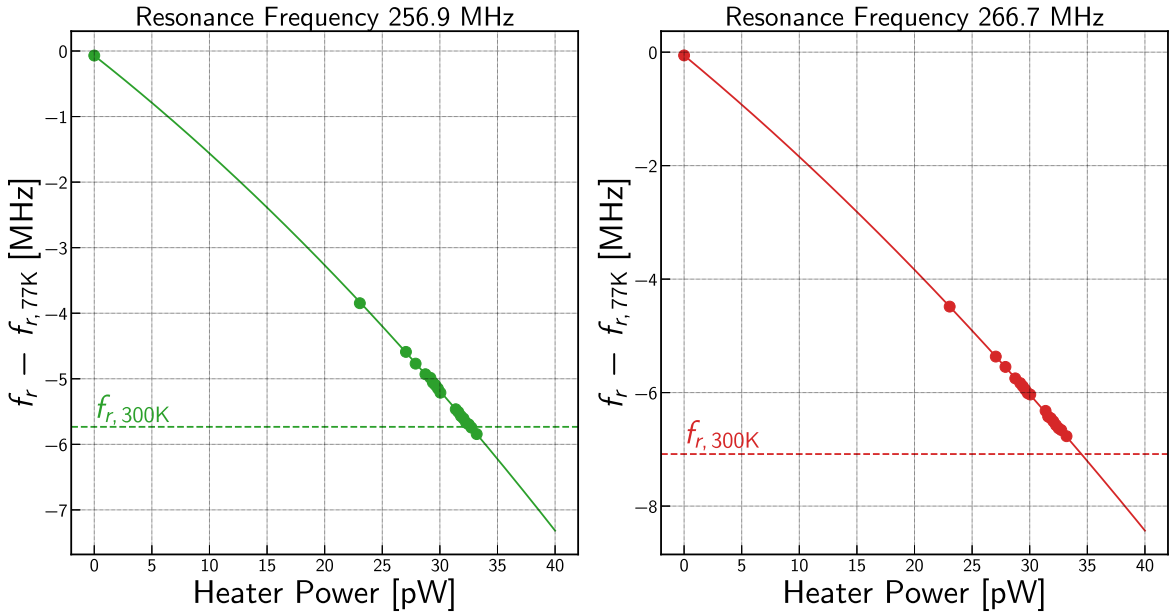

Figure 4: Heater calibrated measurements of the optical efficiency of the 258.5 MHz (left) and 268.8 MHz (right) resonators. The y-axis shows the shift in resonance frequency from the measured frequency under a 77 K optical load. The horizontal dashed line shows the position of the resonance under room temperature loading. The points are discrete measurements of the frequency shift with the heater biased. The solid line is a quadratic fit to the measured frequency versus heater power data that is used to predict ΔP.

4.3 Spectra

Understanding the spectral response of the detectors is crucial in order to constrain potential sources of systematic effects. Such measurements are also required to facilitate component separation of the CMB polarized signal from the dust and

f_r [MHz]	dP/dT [pW/K]	η	ν_0 [GHz]	$\Delta\nu/\nu_0$
258.5	0.15	0.28	150.4	0.26
268.8	0.15	0.30	148.5	0.29
234.2	-	0.26	148.1	0.28
243.1	-	0.35	146.8	0.29

Table 2: Measured optical parameters of the 4 antenna-coupled TKIDs. For the 258.5 MHz and the 268.8 MHz resonators, the optical efficiency was directly measured using the heaters on the bolometer island. For the 234.2 MHz and the 243.1 MHz resonator, the efficiency was computed from the measured spectra assuming that the devices had the same dP/dT as measured on average. The bandcenter ν_0 and bandwidth ν_0 were obtained from the measured spectra of each of the resonators.

synchrotron foreground components which have a different spectral signature.[19] The spectra are primarily determined by the band-defining filter between the antenna and bolometers, but also include roll-off of the antenna, transmission spectra of optics above the focal plane, and any fringing associated with pairs of impedance mismatched interfaces.

To measure the device bandpass, we used a Martin-Pupplet Fourier Transform Spectrometer (FTS) that was mounted on top of the cryostat. In a time reversed sense, the detector beam is split into two beams at the input polarizing beam splitter; with one beam terminating at a 77 K blackbody source made of liquid nitrogen soaked Eccosorb HR-10 and the second beam terminating on an Eccosorb HR-10 blackbody at room temperature. The interference pattern generated as the position of the movable mirror is changed and the interferogram encodes the spectral response of the detectors. The FTS is on a movable x-y stage and is adjusted to find the point of maximum illumination of the detectors. We orient the FTS at a 45° angle to the polarization axes so detectors measuring both polarizations can be simultaneously illuminated. The test chip centered on the focal plane is small enough to illuminate all the detectors at without changing the FTS position on the x-y stage.

All the interferograms are filtered using a moving average filter and aligned at the point of zero path difference before being stacked and averaged. The real part of the Fourier Transform of the averaged interferogram then gives the spectral response of the detector. Figure 5 shows the averaged interferogram and resulting spectrum for the 234.2 MHz resonator. The band center and bandwidth of the detectors are then estimated from the spectra $S(\nu)$ using the relations

$$\nu_0 = \int \nu S(\nu) d\nu \tag{2}$$

$$\Delta\nu = \frac{\left(\int S(\nu) d\nu\right)^2}{\int S^2(\nu) d\nu} \tag{3}$$

Table 2 shows the measured band center and bandwidth for all 4 resonators. Averaged over the 4 detectors, the band center is 148.5 $\pm$ 1.3 GHz and the fractional bandwidth is 28% $\pm$ 1%. As designed, the resonator band avoids the atmospheric oxygen line at 118 GHz and the water line at 183 GHz.[20] There are fringes present in the band with an average standing wave ratio (SWR) of 1.26 $\pm$ 0.06 averaged over all the detectors and the 140-160 GHz range. Using this SWR with a Fabry Perot reflection model predicts a reflectance $R = 0.058 \pm 0.025$, consistent with the expected 4% reflectance from each of the lens surfaces. With new optics coated for the 150 GHz band, we therefore anticipate that the spectra will improve.

5. CONCLUSIONS AND FUTURE WORK

In this proceedings, we present the initial results from our antenna-coupled TKID design. These results establish that we can use standard lab techniques to characterize TKID bolometers designed to observe the CMB at 150 GHz. We also demonstrate that calibration heaters can be used in conjunction with blackbody sources at different temperatures to measure the optical efficiency of TKID detectors.

Using these results, we have designed and are currently fabricating a 4 inch TKID tile with 128 detectors to be installed in a *Keck* telescope at the South Pole. The detectors are tightly packed in an 8x8 array with all the calibration heaters on a single row connected in parallel. The focal plane will hold 4 tiles for a total of 512 detectors on the focal plane. This test camera is planned to deploy in the 2021-2022 Austral summer.

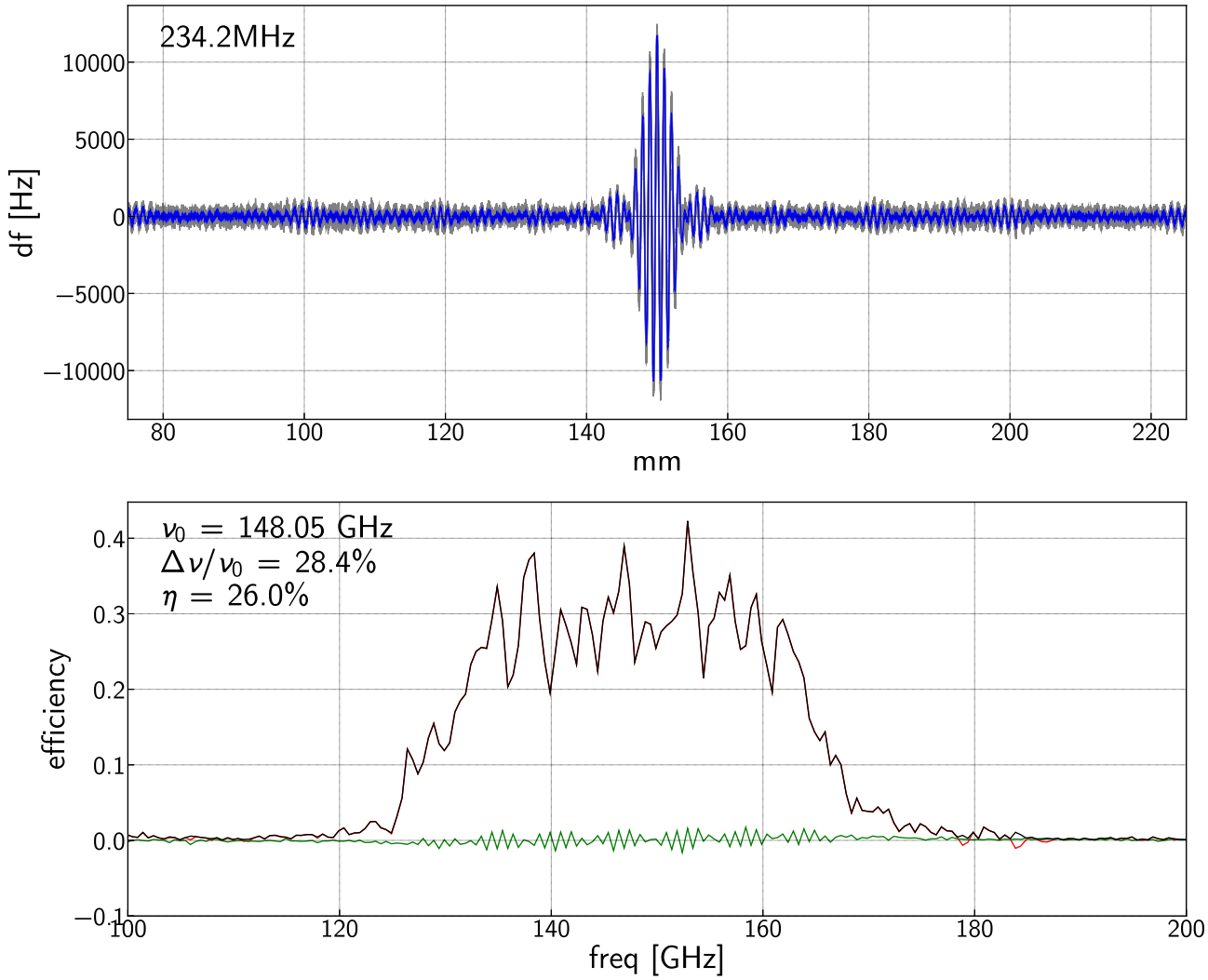

Figure 5: The averaged interferogram (top) and spectrum of the 234.2 MHz resonator (bottom). The blue interferogram is the averaged detector response with the individual interferograms in grey. In the lower plot, the magnitude of the spectrum is shown black with the real part in red and the imaginary part in green.

6. ACKNOWLEDGMENTS

The research was carried out at the California Institute of Technology and the Jet Propulsion Laboratory (JPL), California Institute of Technology, under contract with the National Aeronautics and Space Administration. We acknowledge the JPL Research and Technology Development (RTD) program (2016-19) for strategic support for TKIDs & readout, the President Director Funds, 2018-2020, the NASA SAT: started 2020 (JPL) and the Moore Foundation (started 2019) for funding at Caltech.

7. REFERENCES

[1] Planck Collaboration, Ade, P. A. R., Aghanim, N., Armitage-Caplan, C., Arnaud, M., Ashdown, M., Atrio-Barandela, F., Aumont, J., Baccigalupi, C., Banday, A. J., Barreiro, R. B., Battaner, E., Benabed, K., Benoît, A., Benoit-Lévy, A., Bernard, J.-P., Bersanelli, M., Bielewicz, P., Bobin, J., Bock, J. J., Bond, J. R., Borrill, J., Bouchet, F. R., Bridges, M., Bucher, M., Burigana, C., Cardoso, J.-F., Catalano, A., Challinor, A., Chamballu, A., Chiang, H. C., Chiang, L.-Y, Christensen, P. R., Church, S., Clements, D. L., Colombi, S., Colombo, L. P. L., Couchot, F., Coulais, A., Crill, B. P., Curto, A., Cuttaia, F., Danese, L., Davies, R. D., de Bernardis, P., de Rosa, A., de Zotti, G., Delabrouille, J., Delouis, J.-M., Désert, F.-X., Diego, J. M., Dole, H., Donzelli, S., Doré, O., Douspis, M., Dupac, X., Efstathiou, G., Enßlin, T. A., Eriksen, H. K., Finelli, F., Forni, O., Frailis, M., Franceschi, E., Galeotta, S., Ganga, K., Giard, M., Girard, D., Giraud-Héraud, Y., González-Nuevo, J., Górski, K. M., Gratton, S., Gregorio, A., Gruppuso, A., Hansen, F. K., Hanson, D., Harrison, D., Henrot-Versillé, S., Hernández-Monteagudo, C., Herranz, D., Hildebrandt, S. R., Hivon, E., Hobson, M., Holmes, W. A., Hornstrup, A., Hovest, W., Huffenberger, K. M., Jaffe, A. H., Jaffe, T. R., Jones, W. C., Juvela, M., Keihänen, E., Keskitalo, R., Kisner, T. S., Kneissl, R., Knoche, J., Knox, L., Kunz, M., Kurki-Suonio, H., Lagache, G., Lamarre, J.-M., Lasenby, A., Laureijs, R. J., Lawrence, C. R., Leonardi, R., Leroy, C., Lesgourgues, J., Liguori, M., Lilje, P. B., Linden-Vørnle, M., López-Caniego, M., Lubin, P. M., Macías-Pérez, J. F., Mandolesi, N., Maris, M., Marshall, D. J., Martin, P. G., Martínez-González, E., Masi, S., Massardi, M., Matarrese, S., Matthai, F., Mazzotta, P., McGehee, P., Melchiorri, A., Mendes, L., Mennella, A., Migliaccio, M., Miniussi, A., Mitra, S., Miville-Deschênes, M.-A., Moneti, A., Montier, L., Morgante, G., Mortlock, D., Mottet, S., Munshi, D., Murphy, J. A., Naselsky, P., Nati, F., Natoli, P., Netterfield, C. B., Nørgaard-Nielsen, H. U., Noviello, F., Novikov, D., Novikov, I., Osborne, S., Oxborrow, C. A., Paci, F., Pagano, L., Pajot, F., Paoletti, D., Pasian, F., Patanchon, G., Perdereau, O., Perotto, L., Perrotta, F., Piacentini, F., Piat, M., Pierpaoli, E., Pietrobon, D., Plaszczynski, S., Pointecouteau, E., Polenta, G., Ponthieu, N., Popa, L., Poutanen, T., Pratt, G. W., Prézeau, G., Prunet, S., Puget, J.-L., Rachen, J. P., Racine, B., Reinecke, M., Remazeilles, M., Renault, C., Ricciardi, S., Riller, T., Ristorcelli, I., Rocha, G., Rosset, C., Roudier, G., Rusholme, B., Sanselme, L., Santos, D., Sauvé, A., Savini, G., Scott, D., Shellard, E. P. S., Spencer, L. D., Starck, J.-L., Stolyarov, V., Stompor, R., Sudiwala, R., Sureau, F., Sutton, D., Suur-Uski, A.-S., Sygnet, J.-F., Tauber, J. A., Tavagnacco, D., Terenzi, L., Toffolatti, L., Tomasi, M., Tristram, M., Tucci, M., Umana, G., Valenziano, L., Valiviita, J., Van Tent, B., Vielva, P., Villa, F., Vittorio, N., Wade, L. A., Wandelt, B. D., Yvon, D., Zacchei, A., and Zonca, A., "Planck 2013 results. x. hfi energetic particle effects: characterization, removal, and simulation," *A&A* **571**, A10 (2014).

[2] Abazajian, K. N., Adshead, P., Ahmed, Z., Allen, S. W., Alonso, D., Arnold, K. S., Baccigalupi, C., Bartlett, J. G., Battaglia, N., Benson, B. A., Bischoff, C. A., Borrill, J., Buza, V., Calabrese, E., Caldwell, R., Carlstrom, J. E., Chang, C. L., Crawford, T. M., Cyr-Racine, F.-Y., De Bernardis, F., de Haan, T., di Serego Alighieri, S., Dunkley, J., Dvorkin, C., Errard, J., Fabbian, G., Feeney, S., Ferraro, S., Filippini, J. P., Flauger, R., Fuller, G. M., Gluscevic, V., Green, D., Grin, D., Grohs, E., Henning, J. W., Hill, J. C., Hlozek, R., Holder, G., Holzapfel, W., Hu, W., Huffenberger, K. M., Keskitalo, R., Knox, L., Kosowsky, A., Kovac, J., Kovetz, E. D., Kuo, C.-L., Kusaka, A., Le Jeune, M., Lee, A. T., Lilley, M., Loverde, M., Madhavacheril, M. S., Mantz, A., Marsh, D. J. E., McMahon, J., Meerburg, P. D., Meyers, J., Miller, A. D., Munoz, J. B., Nguyen, H. N., Niemack, M. D., Peloso, M., Peloton, J., Pogosian, L., Pryke, C., Raveri, M., Reichardt, C. L., Rocha, G., Rotti, A., Schaan, E., Schmittfull, M. M., Scott, D., Sehgal, N., Shandera, S., Sherwin, B. D., Smith, T. L., Sorbo, L., Starkman, G. D., Story, K. T., van Engelen, A., Vieira, J. D., Watson, S., Whitehorn, N., and Kimmy Wu, W. L., "CMB-S4 Science Book, First Edition," *arXiv e-prints* , arXiv:1610.02743 (Oct 2016).

[3] Ade, P. A. R., Aikin, R. W., Amiri, M., Barkats, D., Benton, S. J., Bischoff, C. A., Bock, J. J., Brevik, J. A., Buder, I., Bullock, E., Davis, G., Day, P. K., Dowell, C. D., Duband, L., Filippini, J. P., Fliescher, S., Golwala, S. R., Halpern,

M., Hasselfield, M., Hildebrandt, S. R., Hilton, G. C., Irwin, K. D., Karkare, K. S., Kaufman, J. P., Keating, B. G., Kernasovskiy, S. A., Kovac, J. M., Kuo, C. L., Leitch, E. M., Llombart, N., Lueker, M., Netterfield, C. B., Nguyen, H. T., O'Brient, R., Ogburn, R. W., Orlando, A., Pryke, C., Reintsema, C. D., Richter, S., Schwarz, R., Sheehy, C. D., Staniszewski, Z. K., Story, K. T., Sudiwala, R. V., Teply, G. P., Tolan, J. E., Turner, A. D., Vieregg, A. G., Wilson, P., Wong, C. L., and and, K. W. Y., "BICEP2. II. EXPERIMENT AND THREE-YEAR DATA SET," *The Astrophysical Journal* **792**, 62 (aug 2014).

[4] Hui, H., Ade, P. A. R., Ahmed, Z., Aikin, R. W., Alexander, K. D., Barkats, D., Benton, S. J., Bischoff, C. A., Bock, J. J., Bowens-Rubin, R., Brevik, J. A., Buder, I., Bullock, E., Buza, V., Connors, J., Cornelison, J., Crill, B. P., Crumrine, M., Dierickx, M., Duband, L., Dvorkin, C., Filippini, J. P., Fliescher, S., Grayson, J., Hall, G., Halpern, M., Harrison, S., Hildebrandt, S. R., Hilton, G. C., Irwin, K. D., Kang, J., Karkare, K. S., Karpel, E., Kaufman, J. P., Keating, B. G., Kefeli, S., Kernasovskiy, S. A., Kovac, J. M., Kuo, C.-L., Lau, K., Larsen, N. A., Leitch, E. M., Lueker, M., Megerian, K. G., Moncelsi, L., Namikawa, T., Netterfield, C. B., Nguyen, H. T., O'Brient, R., IV, R. W. O., Palladino, S., Pryke, C., Racine, B., Richter, S., Schwarz, R., Schillaci, A., Sheehy, C. D., Soliman, A., Germaine, T. S., Staniszewski, Z. K., Steinbach, B., Sudiwala, R. V., Teply, G. P., Thompson, K. L., Tolan, J. E., Tucker, C., Turner, A. D., Umiltà, C., Vieregg, A. G., Wandui, A., Weber, A. C., Wiebe, D. V., Willmert, J., Wong, C. L., Wu, W. L. K., Yang, E., Yoon, K. W., and Zhang, C., "BICEP Array: a multi-frequency degree-scale CMB polarimeter," in [*Millimeter, Submillimeter, and Far-Infrared Detectors and Instrumentation for Astronomy IX*], Zmuidzinas, J. and Gao, J.-R., eds., **10708**, 1 – 15, International Society for Optics and Photonics, SPIE (2018).

[5] Irwin, K. D. and Hilton, G. C., "Transition-edge sensors," in [*Cryogenic Particle Detection*], Ascheron, C. E., Koelsch, H. J., and Skolaut, W., eds., ch. 3, 63–150, Springer, Berlin, Heidelberg, Heidelberg (2005).

[6] [*The SQUID Handbook*], John Wiley & Sons, Ltd (2005).

[7] Mauskopf, P. D., "Transition edge sensors and kinetic inductance detectors in astronomical instruments," *Publications of the Astronomical Society of the Pacific* **130**, 082001 (jun 2018).

[8] Wandui, A., Bock, J. J., Frez, C., Hollister, M., Minutolo, L., Nguyen, H., Steinbach, B., Turner, A., Zmuidzinas, J., and O'Brient, R., "Thermal kinetic inductance detectors for millimeter-wave detection," *Journal of Applied Physics* **128**(4), 044508 (2020).

[9] Steinbach, B. A., Bock, J. J., Nguyen, H. T., O'Brient, R. C., and Turner, A. D., "Thermal kinetic inductance detectors for ground-based millimeter-wave cosmology," *Journal of Low Temperature Physics* **193**, 88–95 (Nov 2018).

[10] Ade, P. A. R., Aikin, R. W., Amiri, M., Barkats, D., Benton, S. J., Bischoff, C. A., Bock, J. J., Bonetti, J. A., Brevik, J. A., Buder, I., Bullock, E., Chattopadhyay, G., Davis, G., Day, P. K., Dowell, C. D., Duband, L., Filippini, J. P., Fliescher, S., Golwala, S. R., Halpern, M., Hasselfield, M., Hildebrandt, S. R., Hilton, G. C., Hristov, V., Hui, H., Irwin, K. D., Jones, W. C., Karkare, K. S., Kaufman, J. P., Keating, B. G., Kefeli, S., Kernasovskiy, S. A., Kovac, J. M., Kuo, C. L., LeDuc, H. G., Leitch, E. M., Llombart, N., Lueker, M., Mason, P., Megerian, K., Moncelsi, L., Netterfield, C. B., Nguyen, H. T., O'Brient, R., IV, R. W. O., Orlando, A., Pryke, C., Rahlin, A. S., Reintsema, C. D., Richter, S., Runyan, M. C., Schwarz, R., Sheehy, C. D., Staniszewski, Z. K., Sudiwala, R. V., Teply, G. P., Tolan, J. E., Trangsrud, A., Tucker, R. S., Turner, A. D., Vieregg, A. G., Weber, A., Wiebe, D. V., Wilson, P., Wong, C. L., Yoon, K. W., and Zmuidzinas, J., "Antenna-Coupled TES Bolometers used in BICEP2, Keck Array, and SPIDER," *The Astrophysical Journal* **812**, 176 (oct 2015).

[11] Kuo, C. L., Bock, J. J., Bonetti, J. A., Brevik, J., Chattopadhyay, G., Day, P. K., Golwala, S., Kenyon, M., Lange, A. E., LeDuc, H. G., Nguyen, H., Ogburn, R. W., Orlando, A., Transgrud, A., Turner, A., Wang, G., and Zmuidzinas, J., "Antenna-coupled TES bolometer arrays for CMB polarimetry," in [*Millimeter and Submillimeter Detectors and Instrumentation for Astronomy IV*], Duncan, W. D., Holland, W. S., Withington, S., and Zmuidzinas, J., eds., **7020**, 415 – 428, International Society for Optics and Photonics, SPIE (2008).

[12] Ade, P. A. R., Aikin, R. W., Barkats, D., Benton, S. J., Bischoff, C. A., Bock, J. J., Bradford, K. J., Brevik, J. A., Buder, I., Bullock, E., Dowell, C. D., Duband, L., Filippini, J. P., Fliescher, S., Golwala, S. R., Halpern, M., Hasselfield, M., Hildebrandt, S. R., Hilton, G. C., Hui, H., Irwin, K. D., Kang, J. H., Karkare, K. S., Kaufman, J. P., Keating, B. G., Kefeli, S., Kernasovskiy, S. A., Kovac, J. M., Kuo, C. L., Leitch, E. M., Lueker, M., Megerian, K. G., Netterfield, C. B., Nguyen, H. T., O'Brient, R., IV, R. W. O., Orlando, A., Pryke, C., Richter, S., Schwarz, R., Sheehy, C. D., Staniszewski, Z. K., Sudiwala, R. V., Teply, G. P., Thompson, K., Tolan, J. E., Turner, A. D., Vieregg, A. G., Weber, A. C., Wong, C. L., and and, K. W. Y., "bicep2/KECK ARRAY. IV. OPTICAL CHARACTERIZATION AND PERFORMANCE OF THE bicep2 ANDKECK ARRAYEXPERIMENTS," *The Astrophysical Journal* **806**, 206 (jun 2015).

[13] Golwala, S. R., Bockstiegel, C., Brugger, S., Czakon, N. G., Day, P. K., Downes, T. P., Duan, R., Gao, J., Gill, A. K., Glenn, J., Hollister, M. I., LeDuc, H. G., Maloney, P. R., Mazin, B. A., McHugh, S. G., Miller, D., Noroozian, O., Nguyen, H. T., Sayers, J., Schlaerth, J. A., Siegel, S., Vayonakis, A. K., Wilson, P. R., and Zmuidzinas, J., "Status of MUSIC, the MUltiwavelength Sub/millimeter Inductance Camera," in [*Millimeter, Submillimeter, and Far-Infrared Detectors and Instrumentation for Astronomy VI*], Holland, W. S., ed., **8452**, 33 – 53, International Society for Optics and Photonics, SPIE (2012).

[14] Sonnet Software, Inc, "High frequency electromagnetics software, sonnet release 14 user guide," (2013). [Online; accessed 13-January-2020].

[15] Minutolo, L., Frez, C., Steinbach, B., Turner, A., Wandui, A., and O'Brient, R., "Thermal Kinetic Inductance Detectors camera: system level design, strategy and performance forecast," *IEEE Transactions on Applied Superconductivity* .

[16] Swenson, L. J., Day, P. K., Eom, B. H., Leduc, H. G., Llombart, N., McKenney, C. M., Noroozian, O., and Zmuidzinas, J., "Operation of a titanium nitride superconducting microresonator detector in the nonlinear regime," *Journal of Applied Physics* **113**(10), 104501 (2013).

[17] Khalil, M. S., Stoutimore, M. J. A., Wellstood, F. C., and Osborn, K. D., "An analysis method for asymmetric resonator transmission applied to superconducting devices," *Journal of Applied Physics* **111**(5), 054510 (2012).

[18] Zmuidzinas, J., "Superconducting microresonators: Physics and applications," *Annual Review of Condensed Matter Physics* **3**(1), 169–214 (2012).

[19] Hui, H., Ade, P. A. R., Ahmed, Z., Alexander, K. D., Amiri, M., Barkats, D., Benton, S. J., Bischoff, C. A., Bock, J. J., Boenish, H., Bowens-Rubin, R., Buder, I., Bullock, E., Buza, V., Connors, J., Filippini, J. P., Fliescher, S., Grayson, J. A., Halpern, M., Harrison, S., Hilton, G. C., Hristov, V. V., Irwin, K. D., Kang, J., Karkare, K. S., Karpel, E., Kefeli, S., Kernasovskiy, S. A., Kovac, J. M., Kuo, C. L., Leitch, E. M., Lueker, M., Megerian, K. G., Monticue, V., Namikawa, T., Netterfield, C. B., Nguyen, H. T., O'Brient, R., IV, R. W. O., Pryke, C., Reintsema, C. D., Richter, S., Schwarz, R., Sorensen, C., Sheehy, C. D., Staniszewski, Z. K., Steinbach, B., Teply, G. P., Thompson, K. L., Tolan, J. E., Tucker, C., Turner, A. D., Vieregg, A. G., Wandui, A., Weber, A. C., Wiebe, D. V., Willmert, J., Wu, W. L. K., and Yoon, K. W., "Bicep3 focal plane design and detector performance," **9914** (2016).

[20] Karkare, K. S., Ade, P. A. R., Ahmed, Z., Aikin, R. W., Alexander, K. D., Amiri, M., Barkats, D., Benton, S. J., Bischoff, C. A., Bock, J. J., Bonetti, J. A., Brevik, J. A., Buder, I., Bullock, E. W., Burger, B., Connors, J., Crill, B. P., Davis, G., Dowell, C. D., Duband, L., Filippini, J. P., Fliescher, S. T., Golwala, S. R., Gordon, M. S., Grayson, J. A., Halpern, M., Hasselfield, M., Hildebrandt, S. R., Hilton, G. C., Hristov, V. V., Hui, H., Irwin, K. D., Kang, J. H., Karpel, E., Kefeli, S., Kernasovskiy, S. A., Kovac, J. M., Kuo, C. L., Leitch, E. M., Lueker, M., Mason, P., Megerian, K. G., Netterfield, C. B., Nguyen, H. T., O'Brient, R., IV, R. W. O., Pryke, C. L., Reintsema, C. D., Richter, S., Schwarz, R., Sheehy, C. D., Staniszewski, Z. K., Sudiwala, R. V., Teply, G. P., Thompson, K. L., Tolan, J. E., Turner, A. D., Vieregg, A., Weber, A., Wong, C. L., Wu, W. L. K., and Yoon, K. W., "Keck array and BICEP3: spectral characterization of 5000+ detectors," in [*Millimeter, Submillimeter, and Far-Infrared Detectors and Instrumentation for Astronomy VII*], Holland, W. S. and Zmuidzinas, J., eds., **9153**, 1027 – 1037, International Society for Optics and Photonics, SPIE (2014).